PROPELLER TIP VORTEX IMPINGEMENT AND VIBRATORY FORCE ON A RUDDER

Frederick Vernon Minson

PROPELLER TIP VORTEX IMPINGEMENT AND VIBRATORY FORCE ON A RUDDER

by

FREDERICK VERNON MINSON
LIEUTENANT, UNITED STATES COAST GUARD
B.S., United States Coast Guard Academy
(1968)

Submitted in Partial Fulfillment of the
Requirements for the Degree of
Master of Science in Ocean Engineering
and the Degree of
Master of Science in Mechanical Engineering
at the
MASSACHUSETTS INSTITUTE OF TECHNOLOGY
MAY 1974

PROPELLER TIP VORTEX IMPINGEMENT AND VIBRATORY FORCE ON A RUDDER

by

Frederick Vernon Minson

Submitted to the Department of Ocean Engineering and to the Department of Mechanical Engineering on May 10, 1974 in partial fulfillment of the requirements for the degree of Master of Science in Ocean Engineering and Master of Science in Mechanical Engineering.

ABSTRACT

This thesis involves an experimental investigation of the phase relationship between the propeller tip vortex impingement and the vibratory force on a rudder.

The experimental tests were performed in the MIT Variable Pressure Water Tunnel on a spade rudder in the wake of a five bladed propeller. The methodology of conducting the tests and obtaining the results is presented. The tests were conducted for various axial separations of the propeller and rudder. Graphical results of the phase, amplitude, moment, phase of the moment, and the centroid of the vibratory force are presented.

Thesis Supervisor: Dr. Justin E. Kerwin
Professor of Naval Architecture

Department Reader: Dr. Ain A. Sonin
Professor of Mechanical Engineering

ACKNOWLEDGEMENT

The author would like to express his appreciation for assistance, support, and advice throughout this project to Dr. Justin E. Kerwin, Professor of Naval Architecture, whose proposal initiated this project; and to Dr. Ain A. Sonin, Professor of Mechanical Engineering, for his consultation and advice, and to the San Francisco Foundation for their partial financial support.

Thanks are extended to S. Dean Lewis, Engineer in charge of the Hydrodynamics Laboratory (water tunnel), for his time, effort, and interest given during the experimental investigation; and to Anthony Zolotas, Gordon Graham, and Eddy Alcindor for their assistance in the fabrication and handling of the test equipment; and to Peggy Windle for her perseverance in the typing of this thesis.

TABLE OF CONTENTS

LIST OF FIGURES

LIST OF SYMBOLS

$A, B, A_1, A_2, A_3, A_4, A, \beta$	calibration constants
BX	dynamometer output voltage upper gauge
D	diameter of propeller
C	$\frac{\text{axial clearance}}{\text{propeller diameter}}$
E	modulus of elasticity
FX	dynamometer output voltage lower gauge
I	moment of inertia of cross section
J	advance ration
K_c	$\frac{\text{height of centroid of } K_r \text{ above rudder tip}}{\text{rudder span}}$
K_m	$\frac{\text{moment of } K_r \text{ about rudder tip}}{\rho n^2 D^5}$
K_r	$\frac{\text{force on rudder}}{\rho n^2 D^4}$
X	distance from top of test section
Y	deflection
a	cross section area
n	revolutions per second
ρ	density
u	mass per unit length
ω	frequency (radians per second)

I. INTRODUCTION

Traditionally, the rudders of vessels have been hung on rudder posts that were supported at the top, bottom, and spaced points in between. These supports were attached directly to the hull. Eventually, hulls were shaped to fair into a large skeg (such as on a typical merchant vessel) from which the rudder is supported.

During this century improvements have led to more efficient hull shapes and rudder configurations. Rudders are now hung on posts supported from above only and the rudder is not supported by a skeg (such as found on modern destroyers).

As improvements in rudders progressed, hull shapes were changing to reduce resistance at high speeds. These hulls have a much flatter run in the vicinity of the propller. The power expended to drive these vessles at high speeds has greatly increased. To transmit the power, the propeller loading has also increased, thus increasing the magnitude of the unsteady velocities in its wake. To increase control and maneuverability of vessels at slow speeds, spade rudders are now placed in the wake of the propeliers.

The vibratory force on a rudder is of interest for two reasons. First, the vibrations of the rudder are transmitted through the rudder post to the hull. This places additional loa l on the rudder bearings. These transmitted vibrations are a source of excitation to the structure and plating of the hull, Hulls are such complex structures that the entire hull and its parts have many modes of natural vibrations and many natural frequencies. Exciting any of these natural vibrations can shorten the life of parts due to fatigue and increase the noise and discomfort for a habitability consideration. Secondly, the rudder vibrations and excited natural vibrations transmit noise to the ocean. This noise could be a military tactical concern or could mask a device to detect sounds in the ocean.

In the past, there has been a considerable amount of investigation about propellers and their wakes and about rudder forces. There has been very little investigation of propeller excited rudder forces. Frank M. Lewis has conducted tests to measure propeller excited hull and rudder forces. His results are contained in reference (1). To my knowledge, the phase angle between the force and the propeller tip vortex has not been investigated.

This project is an investigation of phase angle between the impingement of the propeller tip vortex and the hydrodynamic vibratory forces on a spade rudder. The propeller used was a five bladed fixed pitch propeller of the general type found on high speed ships. The spade rudder is hung on a rudder post supported from above and not from below. Thus the rudder becomes a cantilever beam which allows more vibratory motion than a rudder which is hung on a skeg supported from below.

The rotation of the propeller creates a wake of unsteady velocity with a period associated with blade frequency. This unsteady velocity causes unsteady lift and drag forces on the rudder. These forces can be resolved into a steady state component and an oscillating component. This project investigates the oscillating component in the lift direction.

Of particular interest is the phase angle between the propeller tip vortex impingement on the rudder and the oscillating component of the lifting force. Also of interest are the amplitude, moment, phase of the moment, and centroid of the oscillating force. Each of these parameters is presented graphically in relation to the axial separation between the rudder and propeller.

II. METHODOLOGY

The purpose of the test was to examine the relationship between the impingement of the propeller tip vortex and the oscillating component of the lifting force. The propeller tip vortex was detected visually by a strobe light flashing on the trailing tip vortex cavitation, (figure 1.). The force on the rudder was detected by a dynamometer. A digital memory oscillascope was used to compare the dynamometer output with a pulse from the strobe light. The following sections describe each component of the system.

Water Tunnel. The tests were performed at the MIT Hydrodynamics Laboratory. The water tunnel has a 20 inch square test section. The propeller was mounted on a shaft which is driven by an electric motor. Water speeds were created and controlled by an impeller (also driven by an electric motor) located at a distant part of the tunnel. A description of the tunnel facilities is included in Appendix A of reference (2).

Propeller. The propeller used in reference (1) was also used in these tests. It has five blades, a 12 inch diameter, and a 2.3 inch hub diameter. The propeller was mounted on the shaft using a faired propeller nut that extended 2.6 inches downstream of the trailing edge of the blades at the hub. The mounted propeller is shown in figure 1.

Rudder. The rudder used in reference 12 was also used in these tests. The rudder originally had a 10 inch span with a root thickness/chord ratio of .2 and a tip ratio of .1, both having a NACA 66 shape. The sweep of the quarter chord was 11.0 degrees while the taper ratio was 0.60. Prior to use in these tests, the root of the rudder was cut off reducing the span to 8.188 inches, while the tip shape remain squared off. The rudder weighed 17

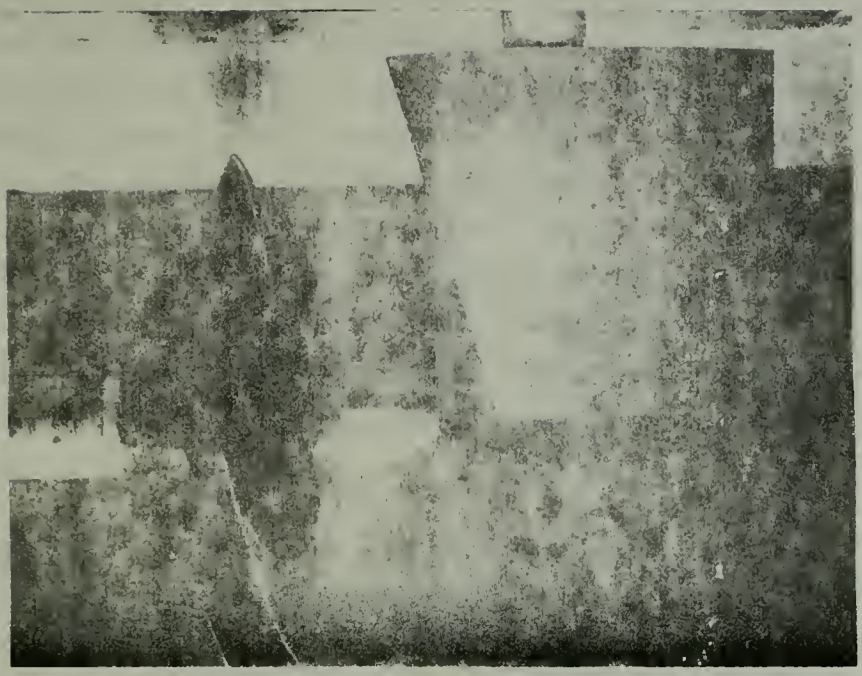

propeller and rudder during data collection

figure 1

pounds. The rudder was mounted rigidly to the dynamometer, approximately on degree to port. The tip of the rudder was located .25 inch below the propeller center line. This rudder placement is not normally found on ships (i.e., not a realistic configuration).

Dynamometer. A description of the dynamometer can be founded in reference (3). The dynamometer has six channels, although only two were used (BX and FX). Both signals originate from strain gauges measuring strain due to bending of the test section in the lift direction. The gauges are located with an axial separation and receive power from an external source (see figure 2). The gauge output was passed through an amplifier within the dynamometer housing and then to a digital memory oscillascope. By static calibration both channels were found to be linear with strain, with the FX channel first to saturate at approximately 80 pounds force at the rudder tip in the lift direction.

Strobe Light. The strobe light was located below the test section flashing through the window in the bottom of the test section. The strobe was triggered from a five tooth wheel on the end of the propeller shaft. The strobe was equipped with an adjustable time delay allowing the strobe flash to coincide with the impingement of each propeller tip vortex. Each flash of the strobe also sent a spike signal to the digital memory oscillascope.

Digital Memory Oscillascope. The signals from BX, FX, and the strobe were processed by a Northern NS-550 Series Digital Memory Oscillascope. The oscillascope had input for four channels to handle up to 100 volts AC or DC. Signals received were sampled at specified time intervals, converted to counts proportional to the sample voltage, and then stored in a digital memory. The sampling starts from a trigger off the same five tooth wheel used by the strobe and takes 254 samples at the specified interval (usually .2

milleseconds). By taking many sweeps of samples and adding corresponding samples, all signals without constant phase with respect to the trigger will add to the average voltage multiplied by the number of sweeps. Signals with constant phase, (trigger frequency or multiples of trigger frequency) will add to the shape of those components of the original signal, but with amplitude multiplied by the number of sweeps. In this manner a record of only these frequencies is stored in the memory along with the number of sweeps sampled. With this timing, the trigger started each sweep on the fourth blade after the previous sweep, thus the signal was the average of the force due to all five blades. This record in memory was then projected on a screen or printed out by a teletype in a series of numbers indicating the number of sweeps and the added value of counts for all the sweeps of 254 samples of each channel. In this manner the voltage signal of BX, FX, and the strobe were all recorded with a common reference time (the trigger).

Natural Frequency Considerations. The dynamometer used was originally designed for measuring unsteady propeller forces. In the event it malfunctioned electrically, had an objectional natural frequency, or was a poor alternative, calculations were made for a rudder mounting using semiconductor strain gauges to detect bending. These calculations were made for various strain levels and two different materials (17-4 PH stainless steel and 5456-T6 aluminum). To achieve the necessary strain levels to have a reasonable gauge output, yet retain sufficiently high natural frequencies to prevent resonance in the desired range, a short thin bending section for the strain gauges is necessary. Natural frequencies were calculated for promising mountings and for the rudder mounted on the existing dynamometer. The method and results are included in Appendix A.

Initial Mounting of Dynamometer. The dynamometer was initially mounted from the top with an 0-ring sealing the tunnel wall penetration. This mounting is shown in figure 2.

Trial Runs and Calibration. Initially a static calibration was performed by applying a known force in the lift direction five and then eight inches below the dynamometer test section. Calibration constants were then computed in the following form:

$$\text{Force} = A(\text{Voltage FX}) + B(\text{Voltage BX})$$

This format was chosen because the force is a function of two linear voltages, therefore superposition (or adding) with the appropriate constants can be used. The calibration was then checked for other forces showing errors of less than five percent.

Next a trial run was conducted for various propeller RPM with a constant J. Forces were expected to vary with the square of the RPM. Instead, the forces decreased to a minimum and then increased rapidly. This appeared to be the effect of natural frequencies.

To investigate the natural frequency of the rudder and dynamometer, the coil and magnet used in reference (1) was obtained. The coil was mounted on the rudder as shown in figure 2. The magnet was mounted from the tunnel wall with its field passing through the coil. Using a signal generator and amplifier, a known force of any desired frequency could be applied to the rudder. By checking the range of frequencies of the trial run, the rudder as mounted had a natural frequency in that range (approx. 90 Hz).

The assumption that the dynamometer was rigid above the test section appeared invalid. Because the rudder and dynamometer could not be altered, various means of mounting the dynamometer

ORIGINAL MOUNTING

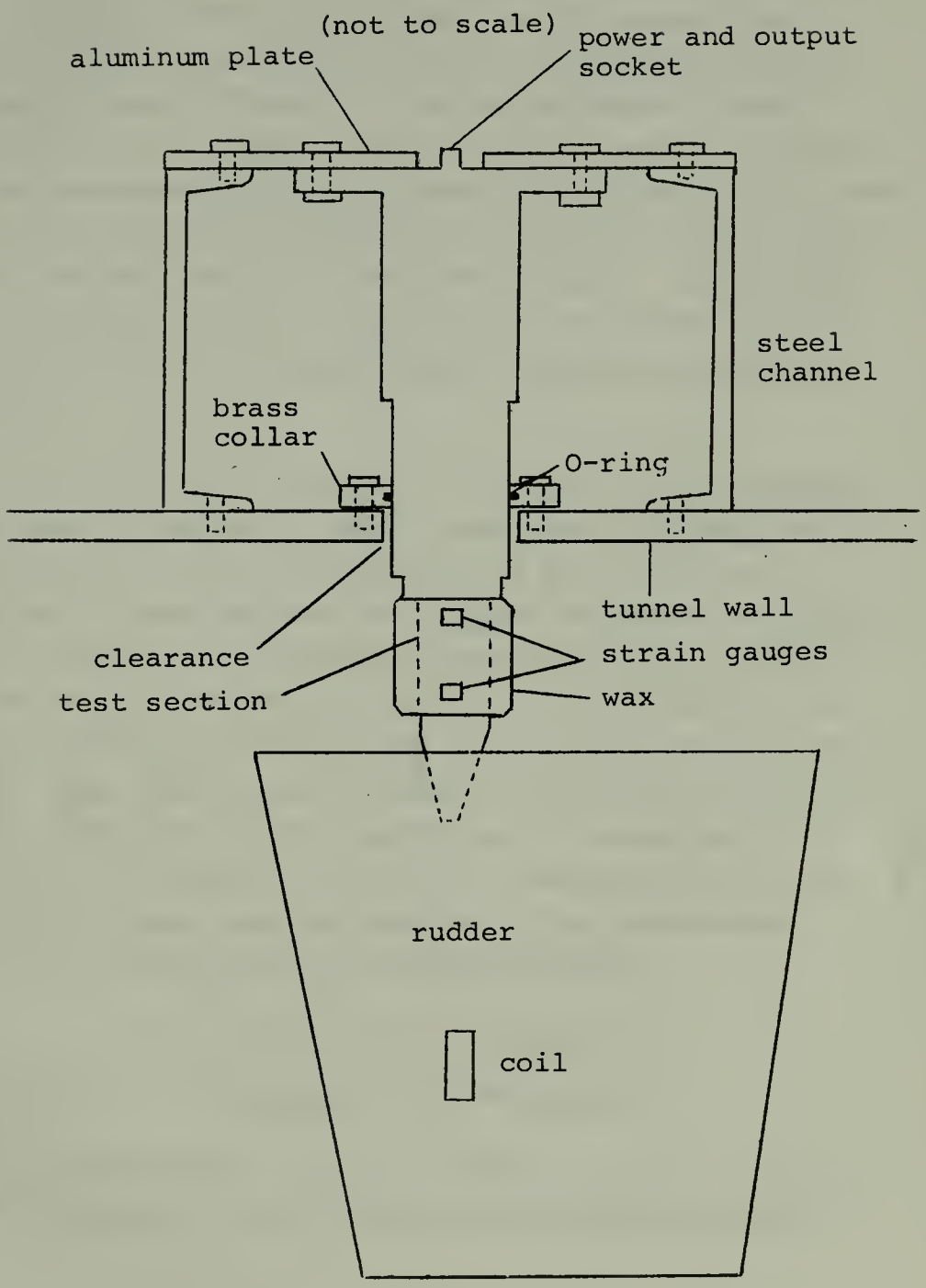

figure 2

were investigated and tried. These methods included mounting rigidly in the middle, top, top and middle, none of which were satisfactory. Also attempted were similar mountings using rubber instead of metal to metal contact between the dynamometer and tunnel wall. Due to a lack of time, the most promising mounting was selected (shown in figure 3). This had the greatest spread between the natural frequency below the desired range (8 Hz with rudder and dynamometer in a mode similar to a pendulum with a node at the top) and the natural frequency above (160 Hz with the mode of a 2 noded vibration similar to a free body in space). Approximate modes were detected with an accelerometer. An added bonus of mounting with rubber was the elimination of essentially all of the tunnel noise.

Because the natural frequency was not sufficiently removed from the range of interest, a dynamic calibration was performed immediately prior to the actual collection of data. This was accomplished by using the same coil, magnet, amplifier, and signal generator. The coil and magnet were mounted as before with the coil located at the bottom of the rudder. A 4.9 ohm high tolerance resistor was placed in series with the coil to measure coil current. From the voltage drop across the resistor the force was calculated. The resistor voltage drop, BX, and FX were processed by the oscillascope and recorded. The phase shift between the force and the strain of the rudder was then tabulated. The dynamometer output was then calibrated by the following equations:

$$\text{Force} = A_1(\text{Voltage FX}) + A_2(\text{Voltage BX})$$

$$\text{Moment} = A_3(\text{Voltage FX}) + A_4(\text{Voltage BX})$$

This format was chosen for the same reasons as the static calibration. These equations were solved by calibrating with the coil at

FINAL MOUNTING

(not to scale)

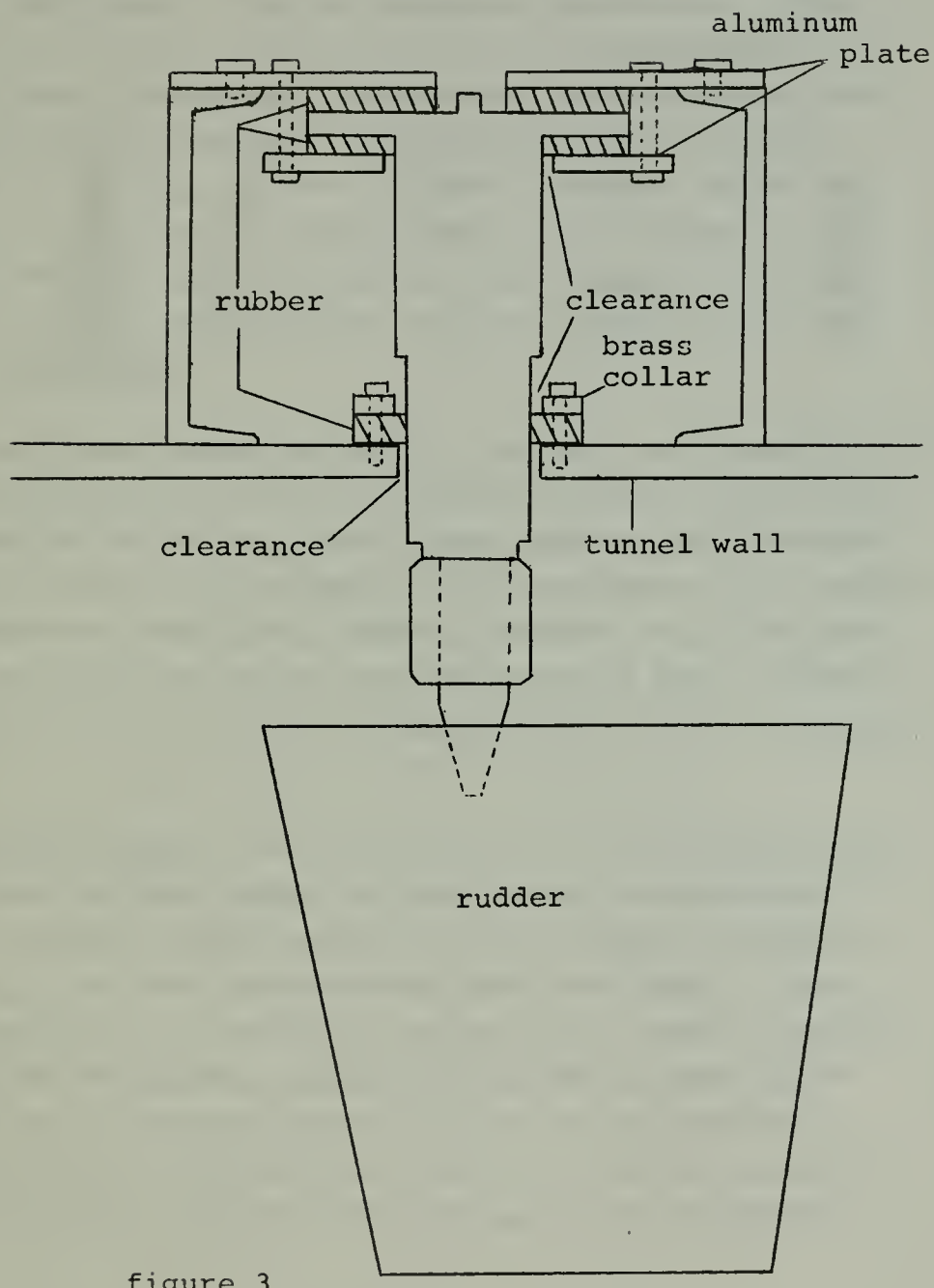

figure 3

the bottom and then the middle of the rudder. The moment reference zero was the rudder tip.

For unknown reasons the calibration points did not show the opposite polarity between FX and BX previously demonstrated in the static calibration. This was considered unreasonable. This was discovered after the data was taken and the dynamometer removed from its mounting. The equipment was reassembled and the calibration was repeated. The points were reasonable and constants A_1, A_2, A_3, A_4 were calculated (constants include both dynamometer characteristics and magnification of rudder motion due to the effect of natural frequency). Small changes were shown to yield very large changes in the constants, therefore, they were considered unreliable.

The problem appeared related to the fact that FX and BX were very small when the coil was in the middle position. Based on the theory that the coil was on or near a node, another calibration was performed with the coil positions at the top and bottom of the rudder. This calibration yielded good constants, changing very little if the calibration points were varied (imitating errors in data). Based on this calibration, the middle coil position was very close to the lower node of the high natural frequency (the two noded mode).

Test Procedure. The test parameters were chosen to yield tip cavitation that was visible, yet small enough to be precisely located. The desired RPM was chosen due to natural frequencies in the drag direction of approximately 50 Hz and 120 Hz. These were considered to be undesirable because a very small crosstalk was observed (during static calibration) between channels of the dynamometer. Minimizing these vibrations yielded an RPM of approximately 910. The water speed was then adjusted to yield the desired tip vortex cavitation while operating at near atmospheric

pressure. The following are the conditions under which the tests were conducted:

Parameter	Value	Tolerance
RPM	910	± 4
Water Speed	6.76 ft/sec	± .04
J	.446	± .005
Pressure (at tunnel ℄)	81.5 cm. mer.	± 1.0
Torque	303 lb.ft.	± 4
Thrust	161 lb.	± 3
Axial Clearance	various	± .002 diameter

Data was collected by first adjusting propeller rudder axial clearance by moving the propeller. Then the strobe time delay was adjusted until the trailing propeller tip vortex cavitation was just separating over the leading edge of the rudder. The digital memory oscillascope would then begin adding the signals of BX, FX, and the strobe pulse. While the signal was added in memory, the memory was viewed on the screen until the signal achieved satisfactory clarity. Finally the teletype would print out the contents of the memory.

On the first run a fourth harmonic of blade frequency of approximately one fourth the amplitude of blade frequency was observed. The series of runs was completed. Then BX and FX signals were passed through Krohn-Hite band pass filters (Model 330B, high cut off 120 Hz, low cut off 2 Hz, at high input, standard peaking) while the series of runs were repeated. Finally, runs were made at several RPM, constant J, and constant axial clearance (both with and without band pass filters).

Because of the fourth harmonic, the repeated and final calibrations were conducted with and without the band pass filters and at the second, third, and fourth multiples of blade frequency. The fourth multiple of blade frequency did show a substantial increase in magnitude indicating that it was near a natural frequency. Calibration with the band pass filters at the multiples of blade frequency showed virtually no output from BX and FX channels after processing by the digital memory oscillascope.

Data Reduction. Data reduction only included applying the calibration to the raw data except for the tests without the band pass filter. Those runs were graphed and then the blade frequency component was estimated.

III. RESULTS

The results of two series of runs is presented in the following graphs. The series are constant J and constant RPM while axial clearance is varied. The phase relationship of the force and moment about the rudder tip with respect to impingement of the propeller tip vortex are present. The force amplitude, moment, and centroid of the force follow. The first series had the dynamometer output passed through the band pass filter before processing by the Digital Memory Oscillascope filter. The second was without filter. The last graph contains the relation between impingement of the tip vortex and the propeller. Figure 4 shows measurements and nomenclature.

Phase. The phase of the force (•) and of the moment (X) with respect to the propeller tip vortex impingement are plotted against axial separation between the propeller axis and the leading edge of the rudder on the shaft centerline (Figure 5). The force and moment phase angles both increase their lead (decrease their lag) with increasing lag. The change is not constant, but appears oscillatory in nature. Figure 6 shows the results of and identical run without filters. Close agreement was found for points E through G.

Force Amplitude. Figure 7 shows force amplitude with filter. The amplitude varies considerably with axial separation. Figure 8 is without filter. The relationship of points D through G is similar to figure 7.

Moment. Figure 9 plots moment with respect to the rudder tip. The shape is similar to figure 6, the force amplitude. Figure 10 is without filter, with no consistent shape.

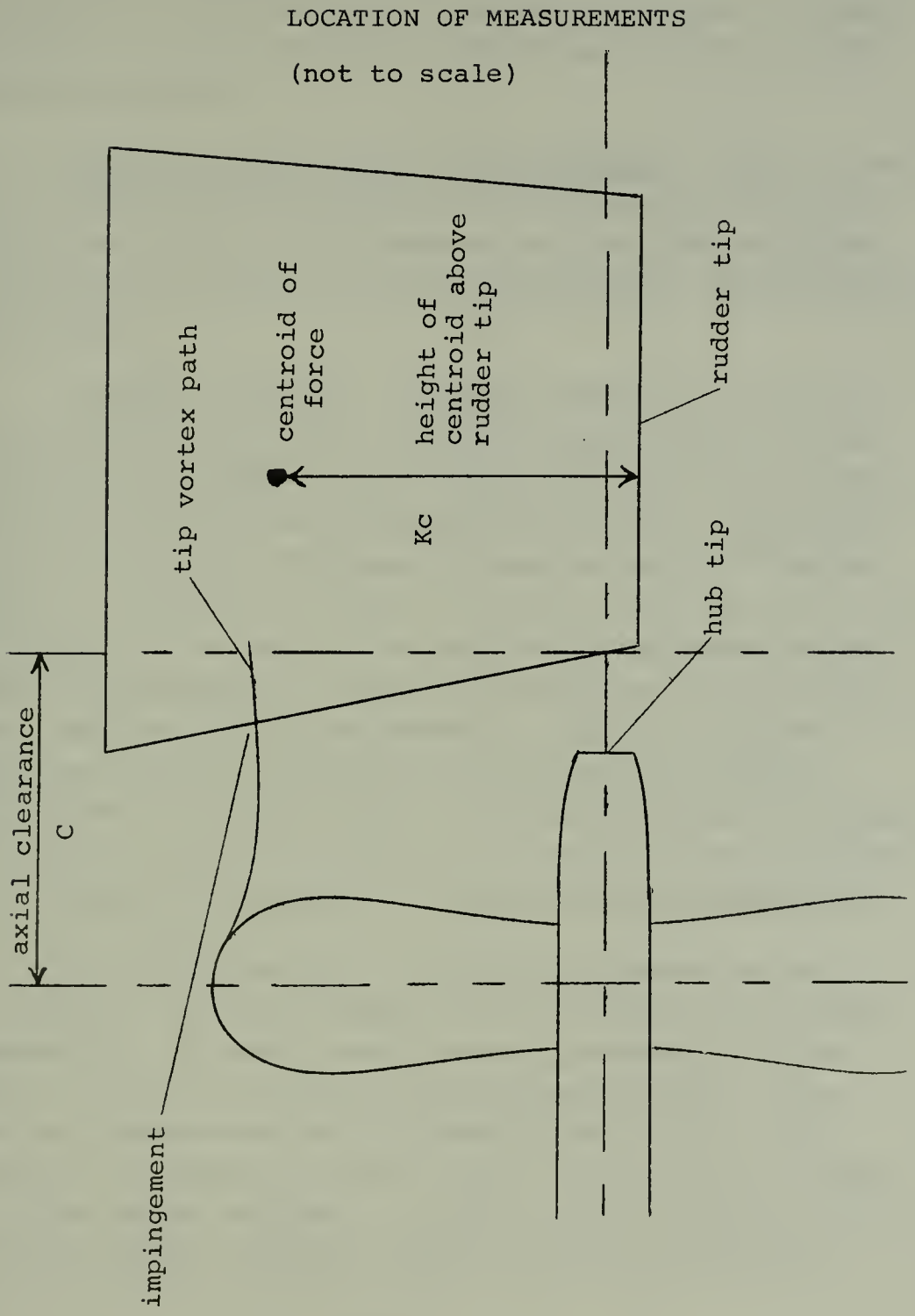
LOCATION OF MEASUREMENTS
(not to scale)
centroid of force
height of centroid above rudder tip
Kc
rudder tip
tip vortex path
hub tip
axial clearance
C
impingement

figure 4

Centroid of Force. Figure 11 shows location of the centroid of the force. With the exception of points F and G there is a consistent pattern. The centroid of the force measured without the filter is widely scattered.

Phase of Propeller Tip Vortex Impingement. Figure 12 plots impingement against axial separation. The phase angle is relative to the propeller but due to the unknown time delay between trigger and sampling of the digital memory oscillascope the reference angle is not known.

Reliability of Results. Agreement between the series with and without the filter is poor. The major cause appears to be the node located in the rudder. Both the accelerometer and the calibrations show a node just above the middle coil position (4.125 inches above the rudder tip). The phase of vibrations shifts 180 degrees when the exciting force is shifted to the other side of the node. The calibration with the coil 4.125 inches above the tip showed that the phase angle changes very little as the exciting force moves near the node. Based on this fact, the reliability of figure 5 is considered good, especially since there was no 180 degree jump indicating that the centroid crossed the node. The shape and slope of the phase of the vibratory force in relation to the propeller was similar to the results presented in reference (1), further indicating creditability.

Because the amplitude of the force and moment are both functions of the difference between FX and BX, precision is needed in measuring. By adding samples over a high number of sweeps (approx. 15,000) the teletype printout has good precision. However, the precision was lost in the data without the filter (due to graphically estimating and subtracting the higher harmonic caused by a higher natural frequency). In addition, the centroid of the force was near the node, resulting in small motions and strains at the

strain gauges. The combined effect of this loss was to reduce the precision of the force and moment measured through the filters and to cause the scatter of the data without the filter (even change the sense of the moment at Points A, B, C, D which accounts for the 180° phase shift). Despite this scatter, whenever the force calculated without the filter was of the right order of magnitude, the phase had close agreement with the results through the filter (points C, D, E, F, G). On all graphs without the filter, points H and I were not plotted because the blade frequency component was completely masked by the higher harmonic.

The shape of the force curve with the filter is similar to the results in reference (1), although the magnitude is questionable due to the proximity of the node. Because the centroid with the filter is reasonable (possible except points E and F) the moments may also have the same shape.

Figure 12 errors are very small. Both runs agreed at all points within 10 degrees. The errors stem from the sources; (1) accuracy of visual adjustment of strobe time delay, and (2) resolution of the digital memory oscillascope (approximately 5 degrees).

Figure 13 shows the shape of the curve for point B without the filter. This was taken with C = 0.381.

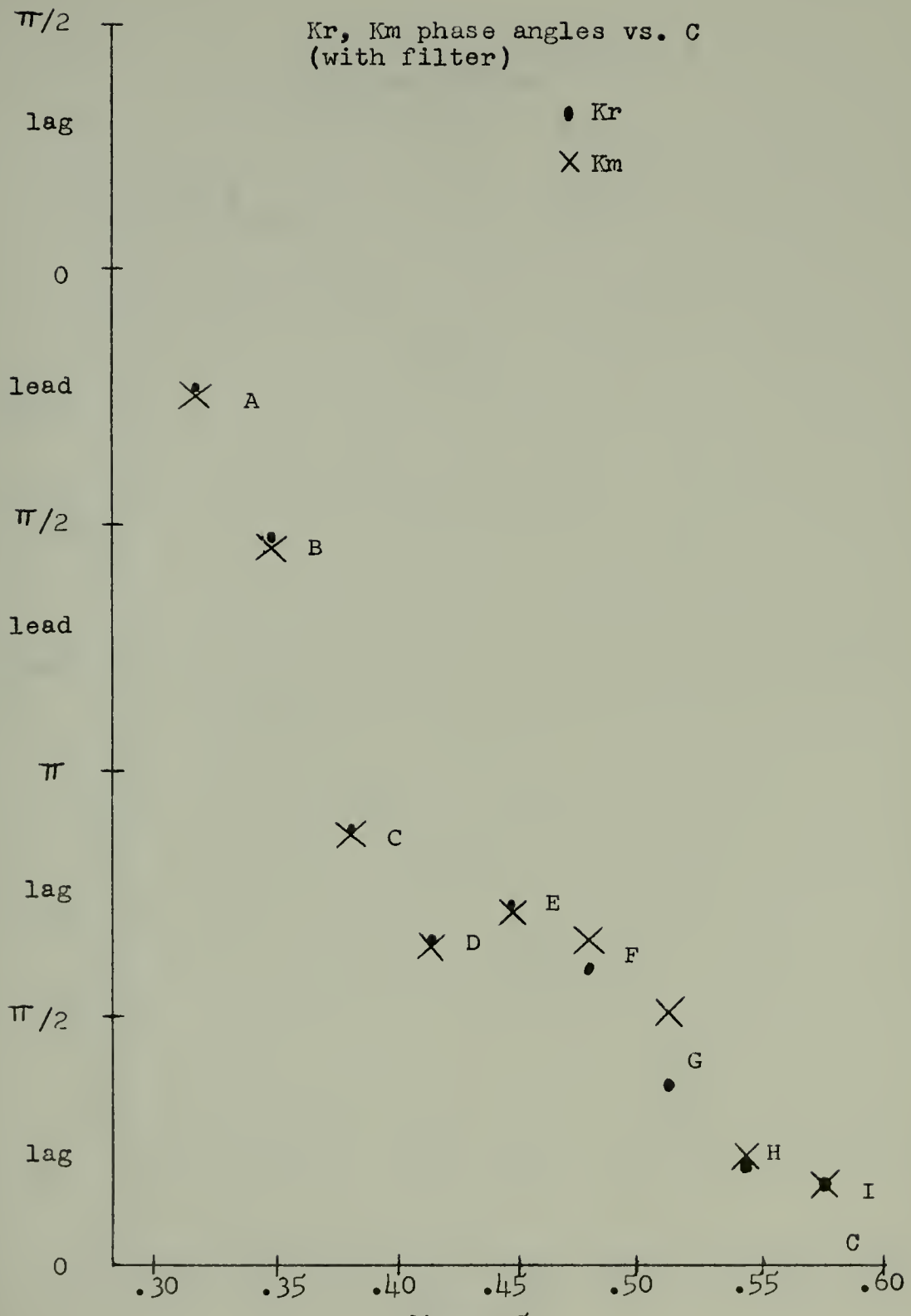
π/2
lag
0
lead
π/2
lead
π
lag
π/2
lag
0
Kr, Km phase angles vs. C
(with filter)
Kr
Km
A
B
C
D
E
F
G
H
I
C
.30
.35
.40
.45
.50
.55
.60

figure 5

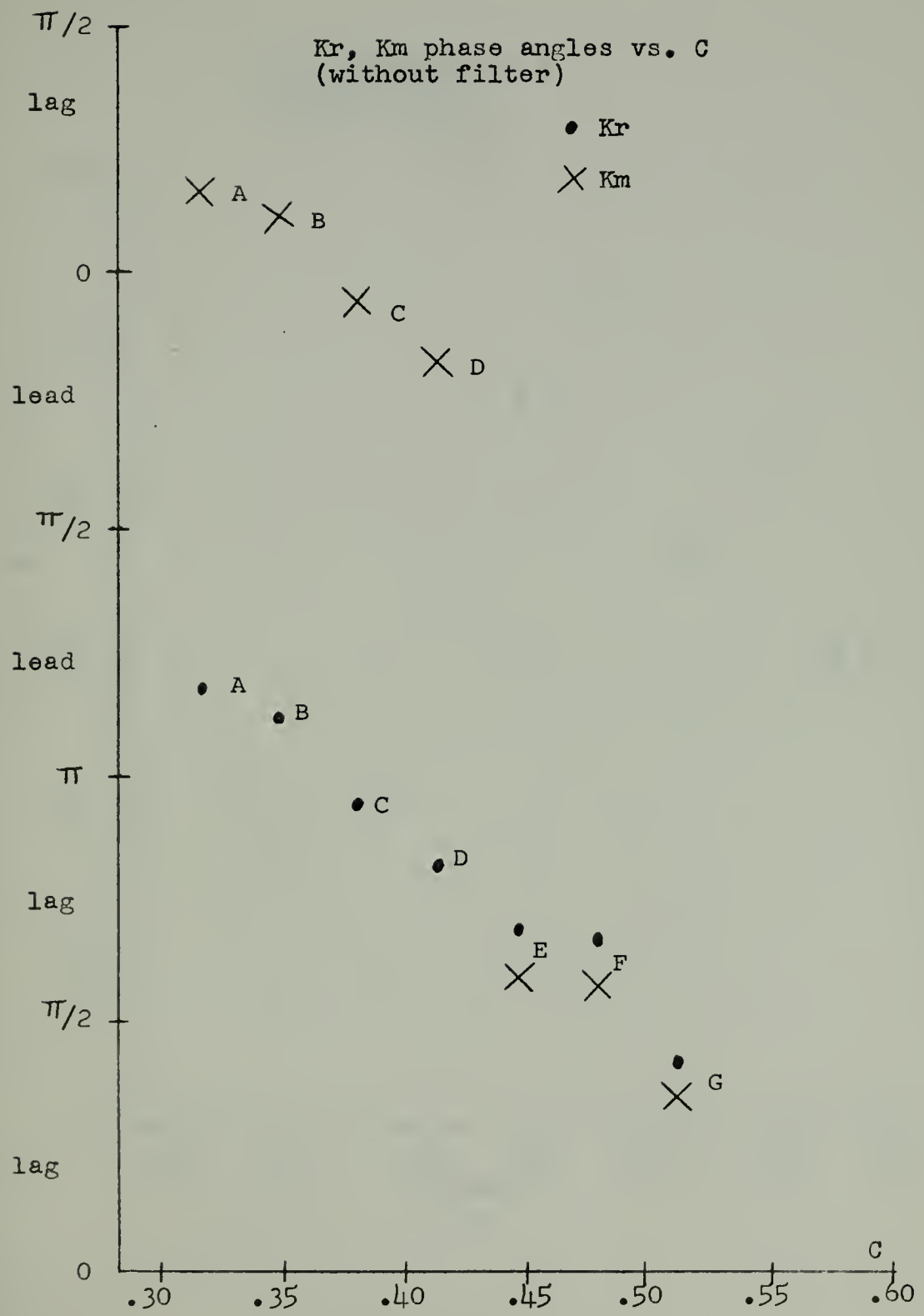
Kr, Km phase angles vs. C
(without filter)
π/2
lag
Kr
Km
A
B
0
C
D
lead
π/2
lead
A
B
π
C
D
lag
E
F
π/2
G
lag
0
C
.30
.35
.40
.45
.50
.55
.60

figure 6

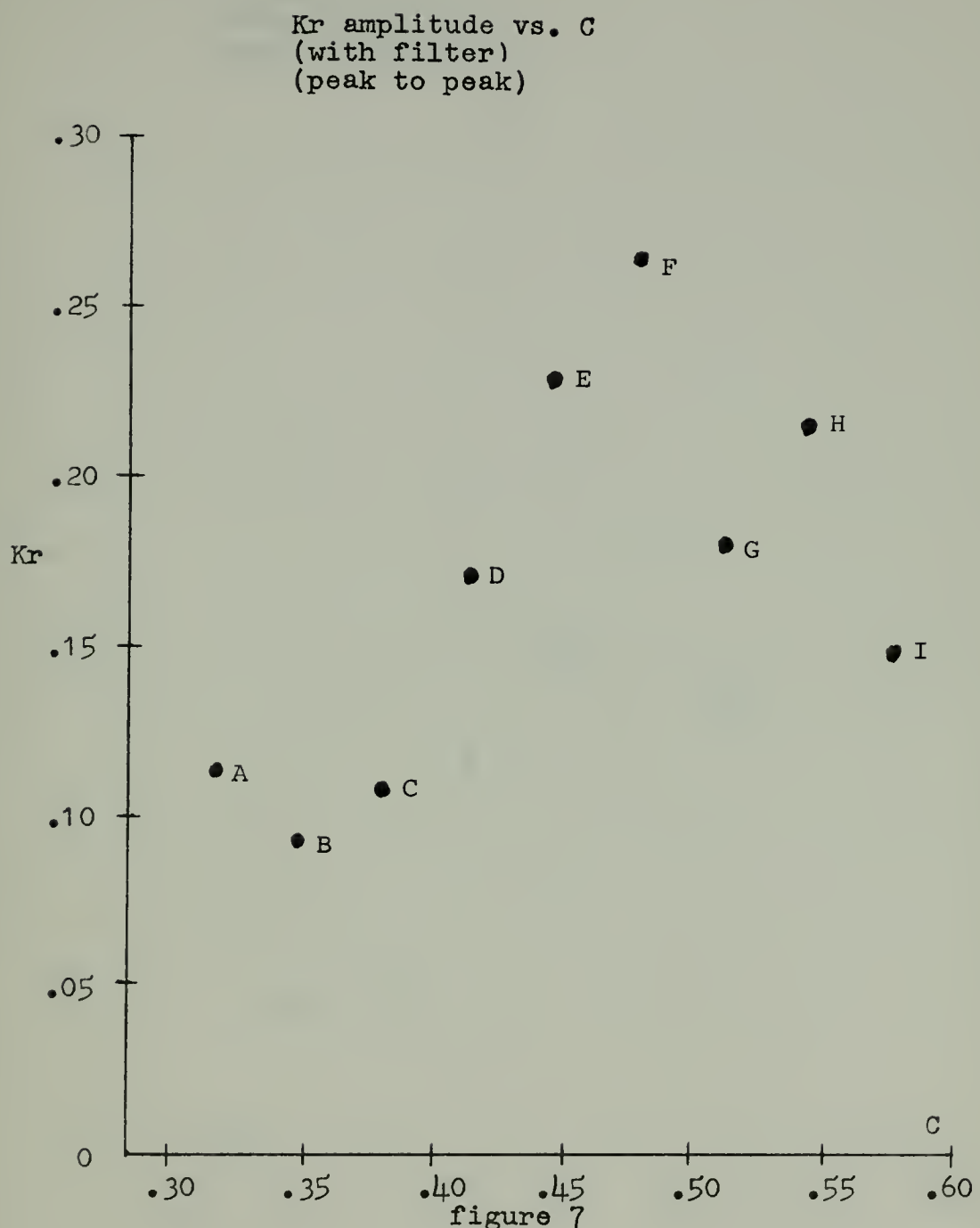
Kr amplitude vs. C
(with filter)
(peak to peak)
.30
.25
.20
.15
.10
.05
0
Kr
A
B
C
D
E
F
G
H
I
.30
.35
.40
.45
.50
.55
.60
C

figure 7

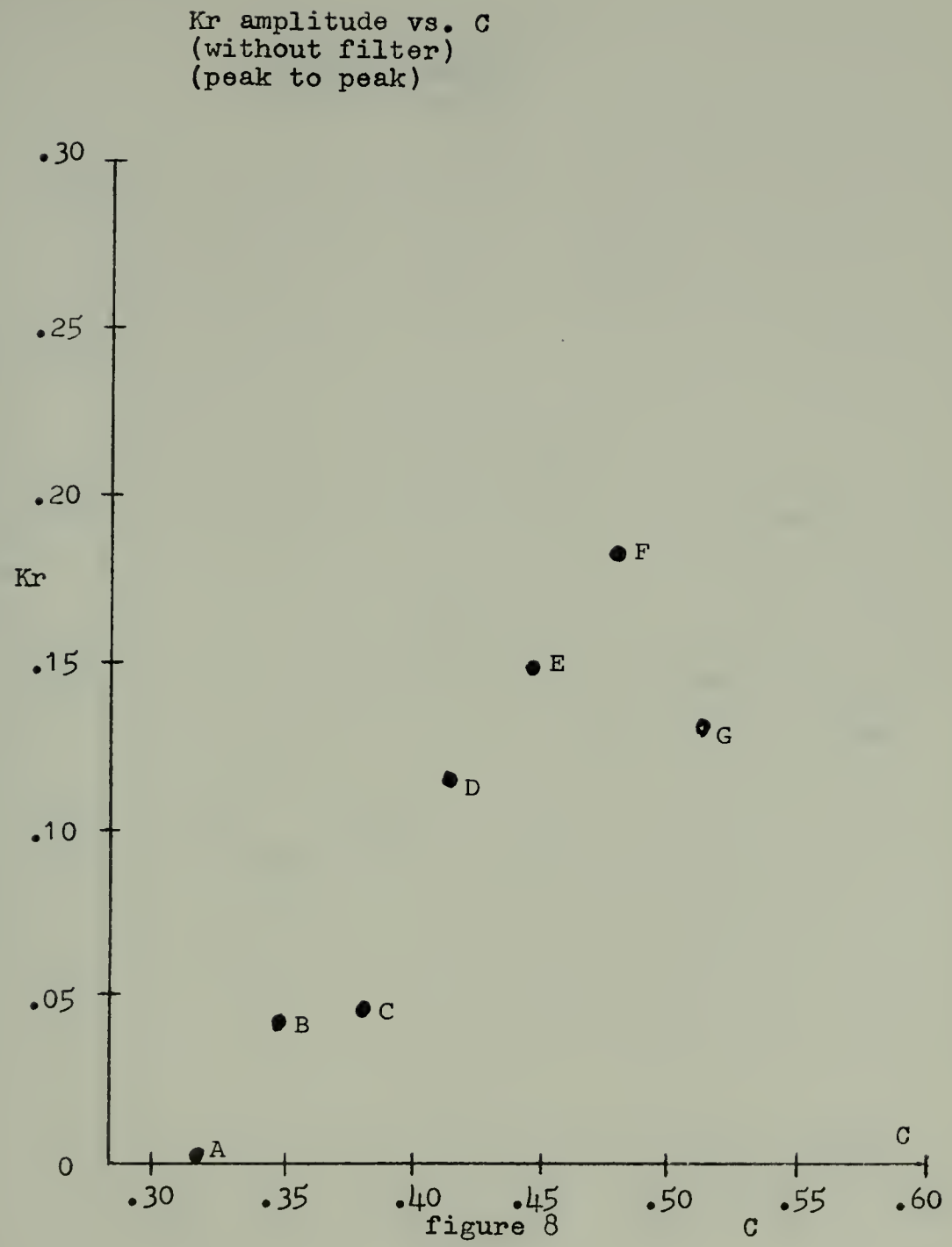
Kr amplitude vs. C
(without filter)
(peak to peak)
.30
.25
.20
Kr
.15
.10
.05
0
A
B
C
D
E
F
G
.30
.35
.40
.45
.50
.55
.60
C
C

figure 8

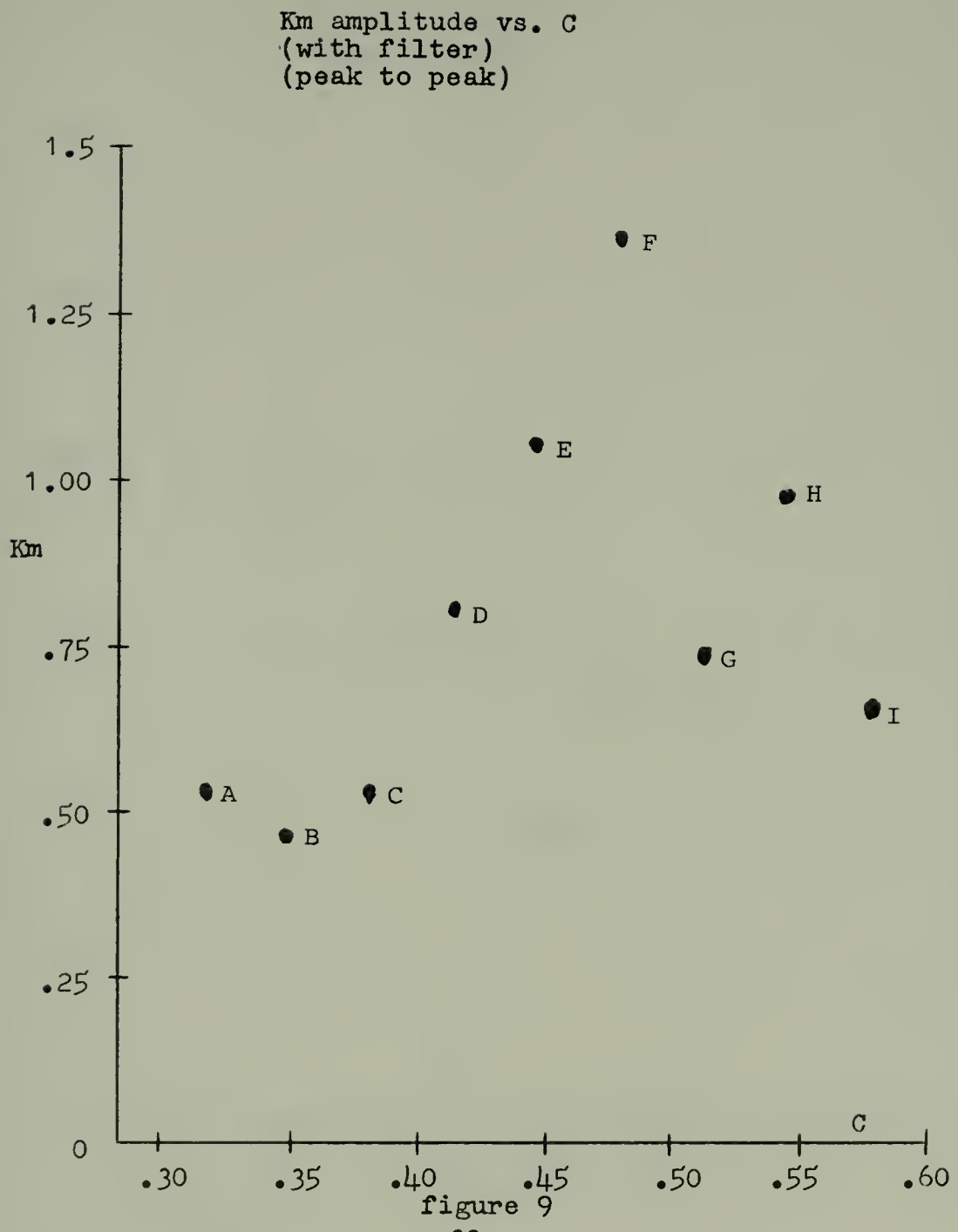
Km amplitude vs. C
(with filter)
(peak to peak)
1.5
1.25
1.00
Km
.75
.50
.25
0
.30
.35
.40
.45
.50
.55
.60
C
A
B
C
D
E
F
G
H
I

figure 9

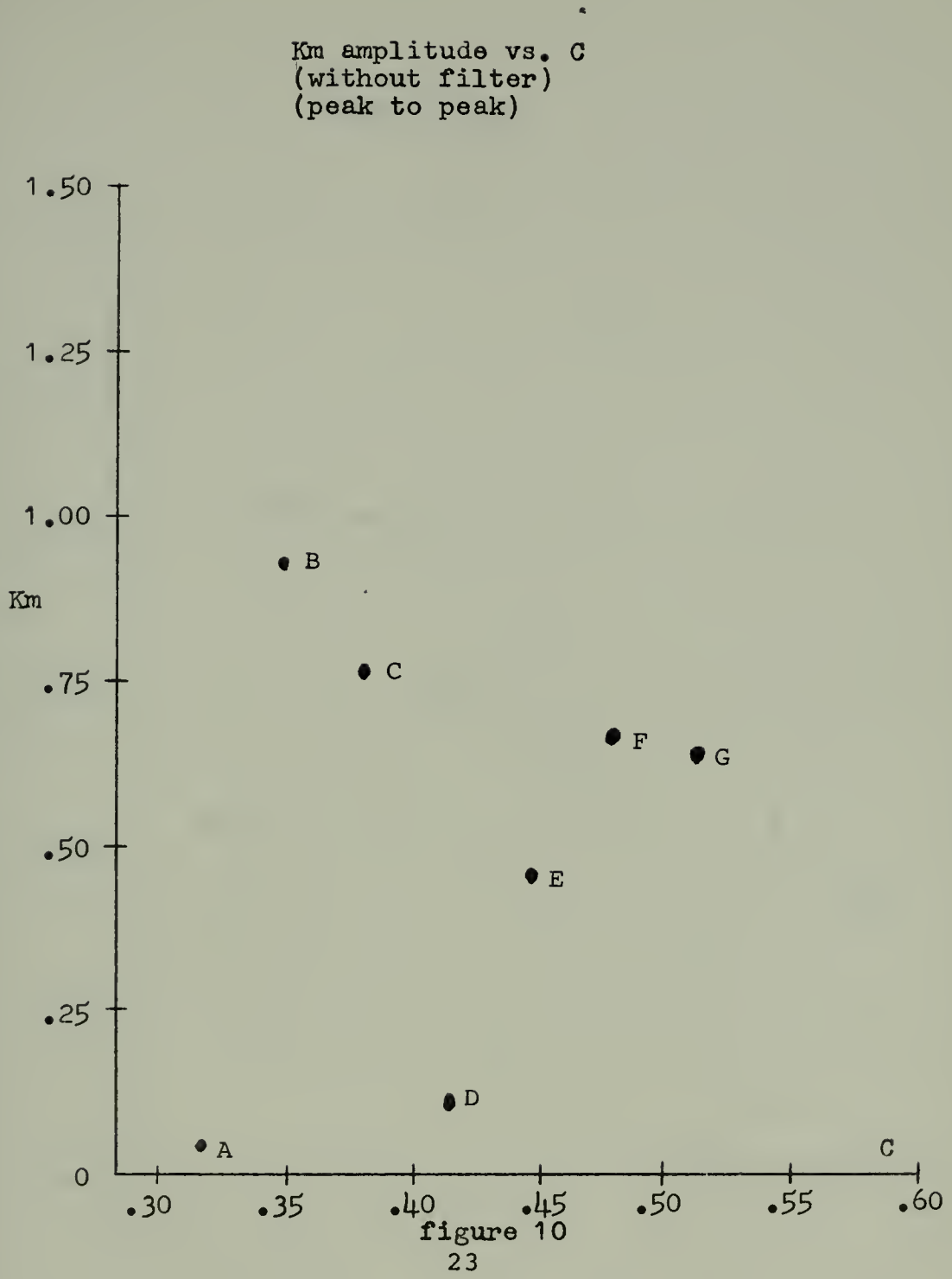
Km amplitude vs. C
(without filter)
(peak to peak)
1.50
1.25
1.00
Km
.75
.50
.25
0
B
C
F
G
E
D
A
C
.30
.35
.40
.45
.50
.55
.60

figure 10

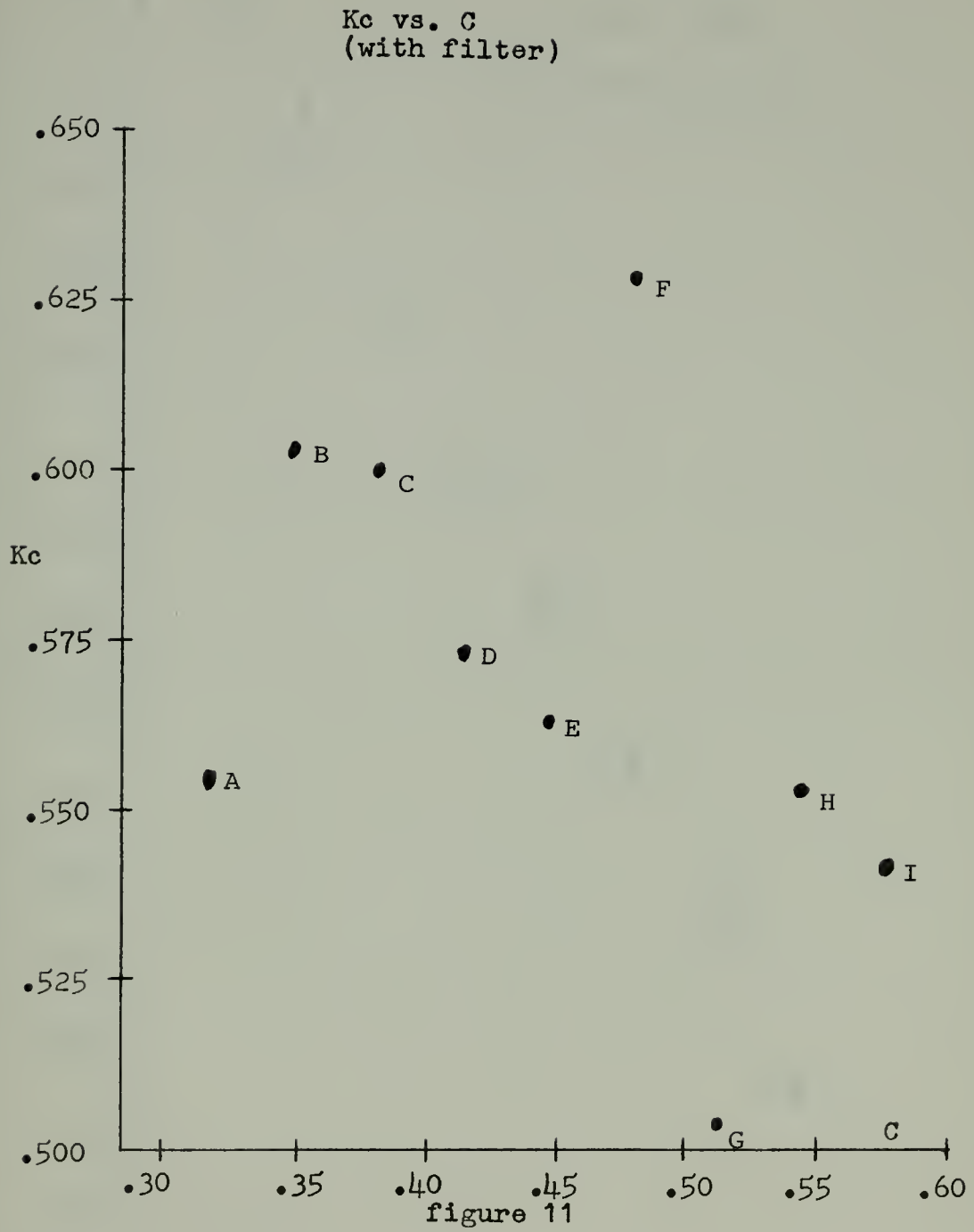
Kc vs. C
(with filter)
.650
.625
.600
.575
.550
.525
.500
Kc
.30
.35
.40
.45
.50
.55
.60
C
A
B
C
D
E
F
G
H
I

figure 11

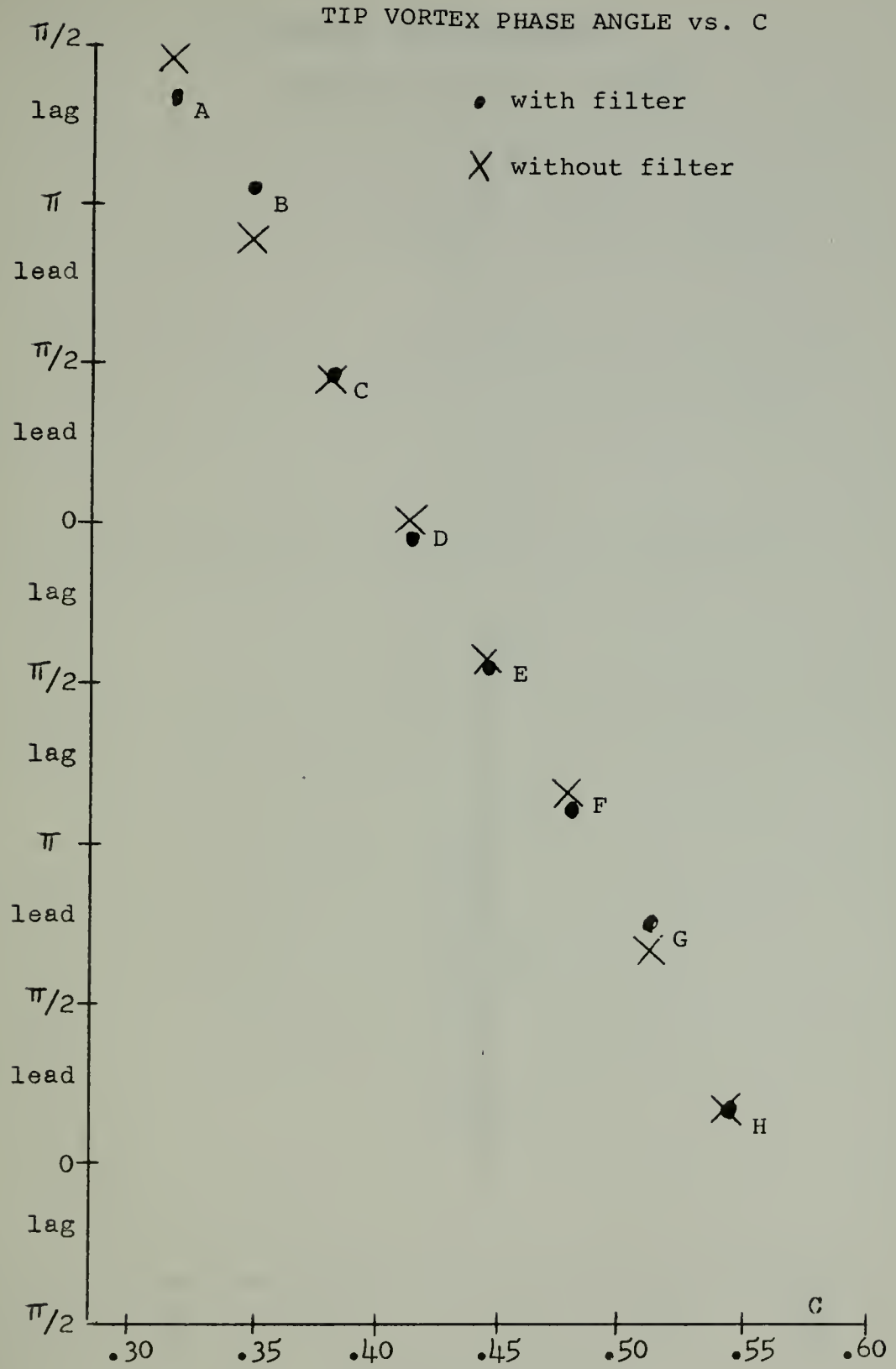
TIP VORTEX PHASE ANGLE vs. C
with filter
without filter
π/2 lag
π lead
π/2 lead
0
π/2 lag
π lead
π/2 lead
0
π/2 lag
A
B
C
D
E
F
G
H
C
.30
.35
.40
.45
.50
.55
.60

figure 12

BX CHANNEL OF DYNAMOMETER

(without filter) C=.381

IV. CONCLUSIONS

This means of measuring the phase relationship between the propeller tip vortex impingement and the hydrodynamic vibratory force on the rudder is feasible. Considerable improvements are needed in the dynamometer mounting to minimize the effect of rudder resonance.

The phase relationship does show a definite increase of the lead of the force. The results of the other parameters have poor accuracy with the use of the filter and are unreliable without the filter.

Further.investigation should proceed when the resonance problem has been eliminated.

V. RECOMMENDATIONS

Many of the problems of this project can be avoided. The problems are essentially vibrational in nature.

Most important is the removal of any natural frequencies from the range of interest. The nearest frequency should be far outside the range of interest. This is also true of higher harmonics.

Secondly, if removal of the natural mode is not possible, take every step to insure that there are no nodes near the centroid of the exciting forces.

Third, increased axial separation of strain gauges in the test section of the dynamometer aids precision, but increasing the length of the test section reduces the natural frequency.

Fourth, when performing a dynamic calibration place the exciting force with the maximum distance between locations. Be sure the exciting force is not near a node.

REFERENCES

1. Lewis, Frank M., "Propeller Excited Hull and Rudder Force Measurements", MIT Report No. 73-10, April 1973.

2. Luckard, Joseph James, "Hydrodynamic Forces and Moments on a Submerged Body of Revolution Resulting from a Fair-water and Control Surfaces", (unpublished Engineers thesis, MIT, 1973).

3. Pfister, William Campbell, "Development of a Procedure to Measure Unsteady Propeller Forces", (Unpublished Masters Thesis, MIT, 1971).

4. Den Hartog, J. P., Mechanical Vibrations, McGraw-Hill Book Company, 1956.

5. Newman, J. N., "Marine Hydrodynamics", second revised edition, MIT, 1972.

6. Allayaud, Donald, "Measurement of Pressure Fluctuations on a Blade Interacting With a Tip Vortex", (unpublished Masters Thesis, MIT, 1968).

7. Baczek, Leonard J., "An Experimental Investigation Concerning Trailing Vortex and Helicopter Rotor Blade Interaction", (unpublished Masters Thesis, MIT, 1970).

8. Chu Sing, "Helicopter Noise Due to Blade/Vortex Interaction", unpublished Masters Thesis, MIT, 1971.

9. Comstock, John P., Ed., Principles of Naval Architecture, SNAME, 1967.

10. Daub, Walter Jacob, "A Flow Visualization Study of the Interaction Between a Trailing Vortex and a Helicopter Rotor Blade, (unpublished Masters Thesis, MIT, 1972).

11. Kerwin, J. E., "Computer Techniques for Propeller Blade Section Design", International Shipbuilding Progress, Volume 20, No. 227, July 1973.

12. Kerwin, J. E., "Experiments on Flapped Rudders Behind a Propeller", (in preparation, Ocean Engineering Dept., MIT).

13. Loukakis, Theodore A., "A New Theory for the Wake of Marine Propellers", MIT Report 71-7, 1971.

14. Tsakonas, S., Jacobs, W. R., Ali, M. R., "Propeller-Rudder Interactions Due to Loading and Thickness Effects", Davidson Laboratory Report SIT-DL-72-1589, Stevens Institute of Technology, 1972.

APPENDIX A

Calculation of Natural Frequency

The natural frequency was calculated by Rayleigh's Method (reference (4)). This method assumes that the shape of deflection is known. It equates the potential energy stored in the deflected shape with the kinetic energy. By this method errors are small when deflection shape is only approximate. In this case, the dynamometer was assumed rigid above the test section. In addition the mass distribution, cross section, and modulus of elasticity must be known.

In this case, the cross section and modulus of elasticity are known. The mass distribution can be calculated from the density and cross section area. Added to this is the additional effect of the mass of water which the rudder accelerates. This was calculated assuming an added mass for an equivalent flat plate, which is equal to the mass of water contained in a circumscribed circle having the rudder chord for a diameter (reference (5)). This was further corrected for the end effects (finite span) by assuming the added mass went linearly to zero between .5 tip chord length above the tip and the tip. This leaves only the shape unknown.

The shape was obtained by a method similar to Stodola (reference (4)). A deflection shape was assumed. Then the following calculations were performed with all integrations by trapazoidal and Simpson's Rule.

$$u = (\rho)(a)$$

$$\text{load} \approx (u)(\text{deflection} = Y)(\text{assumed frequency} = \omega)$$

$$\text{shear} = \int \text{load}\, dX$$

$$\text{moment} = \int \text{shear}\, dX$$

$$Y'' = \frac{\text{moment}}{(E)(I)}$$

$$Y' = \int Y''dX$$

$$Y = \int Y'dX$$

From the new Y, the new deflection, the natural frequency is calculated by Rayleigh's Method. With the new Y and ω, the process is repeated until the new Y has the same shape as the previous Y and the new ω equals the previous ω. Thus the final ω is the natural frequency in radians per second.

The calculations showed that 17-4 PH stainless steel would need a cross section thickness of between .344 and .676 inches for strain ranging from 1/3 to full range of strain permissible on semiconductor strain gauges. Limits for 5456-TG aluminim were .491 to .964 respectively. To obtain larger strain, thinner sections or greater distance from the centroid of the force were needed. However, both of these also lowered the natural frequency. Actual calculations of frequencies for various thicknesses and distances (up to 10 inch practical limit) from the centroid of the force yield frequencies in the 70 to 100 Hz range. The natural frequency of the existing dynamometer and rudder was 270 Hz. Thus the strain level of 30% to 100% of the range of the semiconductor strain gauges is impossible without lowering the natural frequency.

153005
Thesis
M6315 Minson
Propeller tip vortex impingement and vibratory force on a rudder.